Synthesis of SnO$_2$ nanostructures employing Nd:YAG laser

M. Abdul Muhsien[1] · E. T. Salim[2] · Y. Al-Douri[3,4] · A. F. Sale[1] · I. R. Agool[1]

Abstract SnO$_2$ nanostructures have been prepared on quartz and porous silicon (PS) substrates using rapid photothermal oxidation at 600 °C and different oxidation times. The analysis and characterizations were researched. The photovoltage properties of Au/n-SnO$_2$/p-PSi/c-Si solar cell are investigated under irradiation of Nd:YAG laser pulses. The PS is synthesized on single crystalline p-type Si using electrochemical etching in aqueous hydrofluoric acid at current density 25 mA/cm^2 for 30 min etching time. The photovoltage properties are found to be depended on laser flounces.

1 Introduction

Tin dioxide (SnO$_2$) with rutile structure is *n*-type semiconductor with wide band gap ~ 3.6 eV. The structural characteristics of polycrystalline SnO$_2$ are of great importance in various applications such as chemical sensors, solar cells and optoelectronic devices [1–3]. SnO$_2$ has been fabricated using different techniques including electron beam evaporation [4], rf sputtering [5, 6] and chemical vapor deposition [7, 8]. One of the major challenges in synthesizing SnO$_2$ nanostructures is the control over stoichiometry. Since most depositions are carried out in high vacuum condition at high temperatures, SnO$_2$ nanostructures are non-stoichiometric and frequently consist of metastable phases such as SnO and Sn$_3$O$_4$ [9, 10]. The existence of these metastable phases and crystal defects will strongly affect the properties of materials [11, 12]. Therefore, post-deposition annealing in the air is necessary to obtain the stoichiometric SnO$_2$ phase with rutile structure. However, the microstructure of SnO$_2$ nanostructures is mainly controlled by annealing process and number of crystal defects is frequently observed [13, 14]. The structure of SnO$_2$ in its bulk form is tetragonal rutile with lattice parameters $a = b = 4.737$ Å and $c = 3.816$ Å. However, depending on the deposition technique, its structure can be polycrystalline or amorphous. The particle size is typically 200–400 Å, which is highly dependent on deposition technique, temperature and doping level. SnO$_2$ nanostructures close to stoichiometric condition have low free carrier concentration and high resistivity, but non-stoichiometric SnO$_2$ nanostructures have high carrier concentration, conductivity and transparency. This comes from oxygen vacancy in the structure, so the formula is $SnO_2 - x$, where x is the deviation from stoichiometry. Porous silicon (PS) has drawn attention due to its superior properties, required by many applications, as compared to crystalline. PS technology is simple and reliable technology creating nanostructured silicon and advanced material for modern research. PS was discovered by Uhlir [15] who performs electrochemical etching of silicon [16]. It is defined as a composition of silicon skeleton permeated by network of pores, which is formed when the crystalline Si wafers are etched electrochemically in electrolytic solution such as hydrofluoric (HF) acid [17]. The strong visible photoluminescence (PL) [18] and electroluminescence [19] from PS at

✉ Y. Al-Douri
yaldouri@yahoo.com

1 Department of Physics, College of Science, Al-Mustansiriyah University, 35010 Baghdad, Iraq

2 Department of Applied Science, University of Technology, 35015 Baghdad, Iraq

3 Institute of Nano Electronic Engineering, University Malaysia Perlis, 01000 Kangar, Perlis, Malaysia

4 Department of Physics, Faculty of Science, University of Sidi-Bel-Abbes, 22000 Sidi Bel Abbès, Algeria

room temperature have opened new possibilities for Si-based optoelectronic applications [20]. Fabrication and characterization of PS photodetectors by electrochemical etching were reported [21]. Few studies have reported on the effect of laser irradiation on the PL and structural properties of PS [22, 23]. It was mentioned that PL of PS depends on irradiating laser energy density for using in optical recording and storage information on the surface of Si [24].

Ayllon and Lira-Cantu [25] have reported results on the application of SnO_2 thin films in all solid-state hybrid solar cells. They have compared the results with other five solar cells developed in our laboratories applying MEH-PPV and semiconductor oxides like TiO_2, Nb_2O_5, ZnO, CeO_2 or CeO_2–TiO_2. The effects of factors, such as UV light, polymer thickness, stabilization in the dark and performance under irradiation conditions, have been investigated. Open-circuit voltage and short-circuit current values were about −0.45 V and 0.17 mA/cm^2, with fill factors around 30 %. Kersen [26] has studied the synthesis of undoped nanocrystalline tin dioxide powders and the subsequent preparation of SnO_2 thick films. An initial mixture of $SnCl_2$ and $Ca(OH)_2$ was sealed in a vial for milling in an air atmosphere. Heat treatment of the milled powder resulted in the formation of tetragonal and orthorhombic SnO_2 phases, which was confirmed by X-ray diffraction (XRD) analysis. It was found that crystallite size could be controlled by varying the milling time, the rotation speed and the temperature used for the heat treatment. He has obtained crystallite sizes in the range 20–30 nm. And, Omata et al. [27] have prepared indium tin oxide (ITO) and Er^{3+}-doped ITO powders by a conventional ceramic method. The density of ITO powders and optical absorption spectra of Er^{3+} ions in Er^{3+}-doped ITO were measured as a function of the SnO_2 doping level. Their results were discussed in terms of the trapping center for immobile electrons in ITO.

To the best of our knowledge, the effect of laser irradiation on PS photodetector is not available in the literature. In the present work, the effect of pulsed Nd:YAG laser irradiation at different flounces, 20, 30, 40 and 50 mJ/cm^2 at room temperature, on the performance of Au/SnO_2/PS/c-Si heterostructure for solar cell fabricated by electrochemical etching is demonstrated. Analysis and characterization are archived successfully. This work is divided into followings; Section 2 discusses experimental part. The results and discussion are detailed in Sect. 3. And, Sect. 4 presents conclusion.

2 Experimental

Using thermal evaporation technique at room temperature, a high-purity tin (Sn) material was deposited on quartz and porous silicon (PS) substrates. It was performed to use electrochemical anodization in dark to produce PS on polished p-type, single crystal Si (111) wafer with resistivity, 10 Ω-cm. 1:4 mixture of 40 % HF/99 % ethanol was used as an electrolyte [28]. Using current density 25 mA/cm^2 for fixed time 30 min, ionization was carried out. The wafer and platinum cathode were placed in Teflon jig, schematically illustrated in Fig. 1. The samples were rinsed first with pentane, then with 98 % methanol and finally with deionized water 18.5 MΩ. Next, the samples were dried at 60 °C on hot plate rather than drying in N_2 nozzle in order to avoid cracking and peeling of PS layer. The resistivity and type of conductivity of Si substrates were measured by four-point probe (FPP) technique. SnO_2 was obtained with aid of rapid photothermal oxidation system with halogen lamp as oxidation source. The oxidation condition used to form SnO_2 at 600 °C and 90 s oxidation times found to be the best preparation condition from our last work [29]. For the system used to prepare the oxide film, quartz tube of 3 cm diameter with two open ends was used to ensure the flowing of air through it. The source of dry oxygen was used. 650-W halogen lamps were used to provide light, heat radiation and variable power supply to control the output power. k-type thermocouple was used to monitor samples' temperature. Si was used as substrate for TCO's/PS heterojunction. Ohmic contacts were fabricated by evaporating 99.999 % pure aluminum wires for back contact, and 99.999 % pure gold was used as front contact through special mask using Edwards coating system. Boat of tungsten was used to include the evaporated source. Pulsed Nd:YAG laser system type (Guangzhou Huafei Tongda Technology Co., China), providing pulses at 1064 nm wavelength and pulse duration of 10 ns, was used for treatment of Au/SnO_2/PS/c-Si heterostructure at
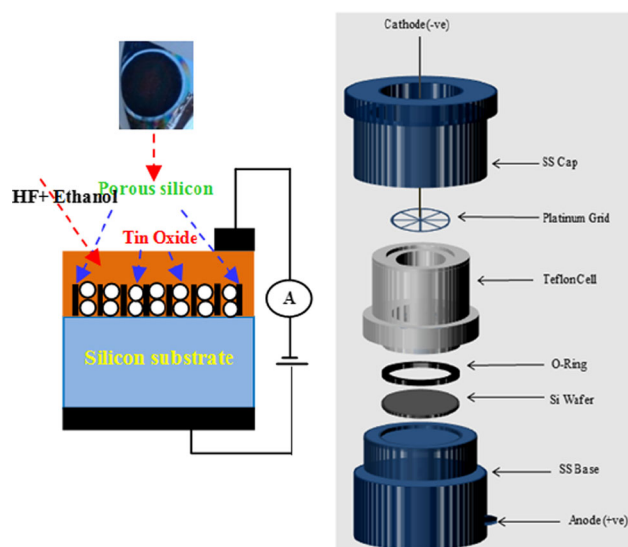
Fig. 1 Schematic illustration of PS etching setup

different flounces, 20, 30, 40 and 50 mJ/cm^2 at room temperature.

3 Results and discussion

Figure 2 illustrates SEM images of PS layer formed on p-type c-Si (111) sample grown at current density 25 mA/cm^2 and fixed time 30 min. The array of void spaces (dark) in silicon matrix (bright) can be seen clearly in the plan view. The morphology shows the electrochemical etching is done uniformly on the surface and created the granular structure in spherical shape. Large number of pores distributed in all direction can be observed in Fig. 2a. Pores with sphere-like appearances were evidently randomly distributed on PS surface. A modest density of pores was observed, and porosity was approximately 85 %. The average pore diameter of PS layer formed on p-type c-Si (111) wafer was 26.41 nm. Figure 2b shows SEM cross-sectional image of PS formed on p- types Si (111). The thickness of PS is increased as porosity increases. The thickest layer was approximately 60.27 μm for p-type c-Si (111).

The porosity ($P\% = 85$ %) and thickness ($t_{PS} = 60.27$ μm) of PS were calculated by measuring the weight of the samples before and after the etching process using Eqs. (1) and (2), via Mettler AE160 digital steelyard with the accuracy of 10^{-4} g was used to weight the samples.

$$P(\%) = \frac{M_1 - M_2}{M_1 - M_3} \tag{1}$$

$$t_{PS} = \frac{M_1 - M_3}{A - D_{Si}} \tag{2}$$

where M_1 is the wafer weight before anodization, M_2 is the weight after anodization, M_3 is the weight after rapid dissolution of whole porous layer in 3 % KOH solution, A is the etched area (cm^2), and D_{Si} is the density of Si in g/cm^3 [30].

The FTIR spectra of porous structure prepared at $J = 25$ mA/cm^2 are shown in Fig. 3, using FTIR spectrometer (Shimadzu FTIR-8400S, Japan) in the range 400–4000 cm^{-1} wave numbers which contains the fundamental vibration frequency of the main bonding including the silica-based ones. The observed FTIR peaks are listed in Table 1. For solar cells application, top layer is required to be lower reflective surface. Photoluminescence (PL) reradiates photons. The excitation to higher energy state then return to lower energy state accompanied by emission of photon is described by PL. PL spectrum of PS is shown in Fig. 4. The peak of emission is observed at 650 nm, and the band gap is 1.91 eV. The reason of increasing PL peak can be understood by quantum confinement mechanism [31, 32]. Based on that, decreasing of Si size with increasing current density is revealed in monotonous blue shift of PL maximum at room temperature. Though, correct interpretation of blue shift of PL spectra requires detailed

Fig. 2 a SEM image of PS, b SEM cross-sectional image of PS formed on p-type c-Si (111)
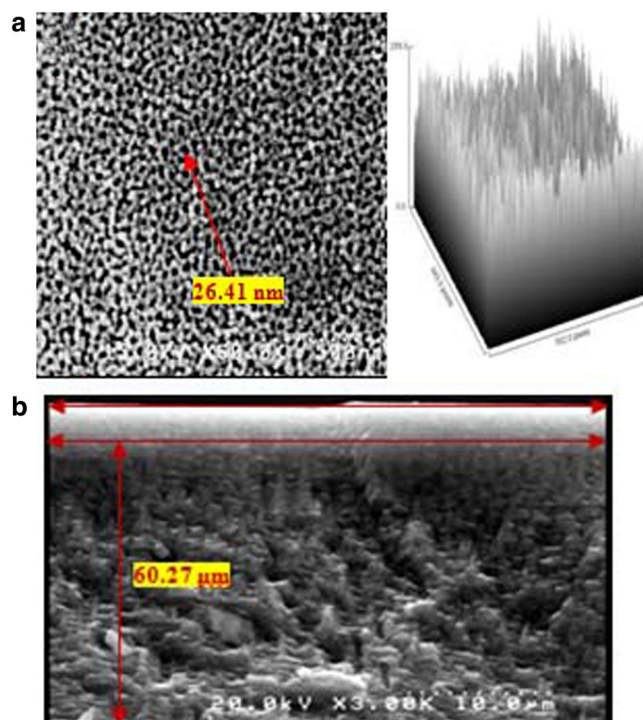
Fig. 3 FTIR spectrum of PS at 25 mA/cm^2 and etching time 30 min
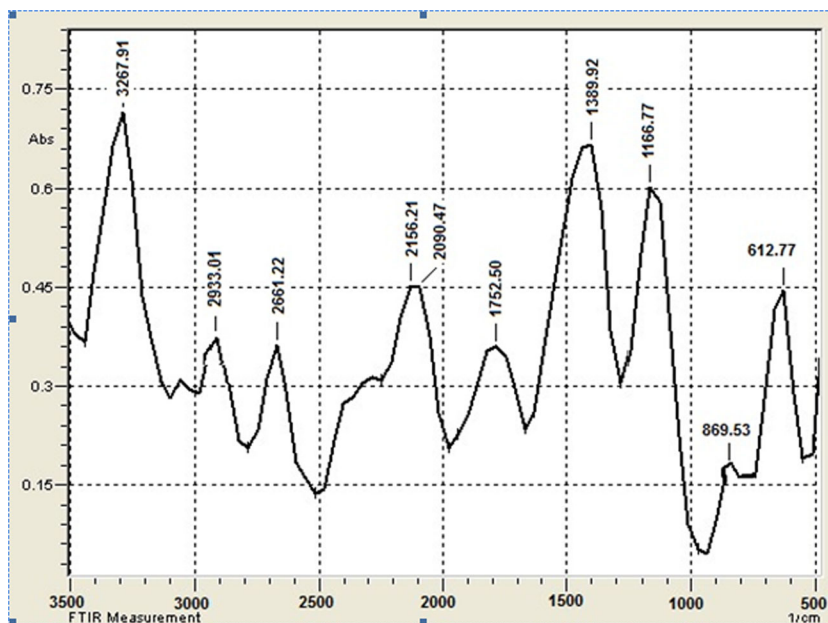
Table 1 FTIR peaks observed in several PS FTIR measurements

Absorption band (cm^{-1})	Mode	Vibrational mode
612.77	Si–Si	Stretching
869.53	Si–H$_2$	Wagging
1166.77	Si–O	Stretching in O–Si–O
1752.50	C=O	Carbon oxygen bond
2090.47	Si–H	Stretch Si$_3$–SiH
2156.21	Si–H	Stretching Si$_2$H–SiH
2933.01	C–H	Asymmetric stretching (CH$_2$)
3267.91	OH	Stretching, water vapor

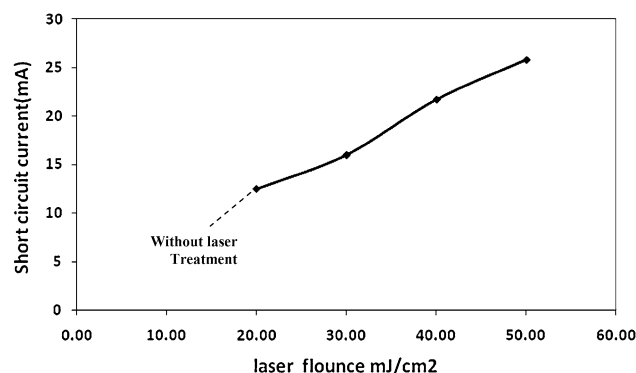**Fig. 4** PL spectrum of PS at 25 mA/cm^2 and etching time 30 min

knowledge of PS morphology. The PL analysis is useful for designing the nanoscale optical band gap device.

Figures 5 and 6 show the short-circuit current and open-circuit voltage, respectively, at different laser flounces and AM1 light intensity of about 100 mW/cm^2; a significant enhancement could be recognized. This enhancement is directly related to the recrystallization of SnO$_2$ nanostructures resulted in enhancement of morphology that reflects in new defect-free structure, which results in higher current and voltage produced per incident photon flux.

The current–voltage characteristics of solar cells were examined under 100 mW/cm^2 illuminations. The relationship between I_{SC} and V_{OC} as a function of load resistance could be recognized in Fig. 7. The efficiency of Au/SnO$_2$/PS/c-Si heterostructure has been measured in five cases for comparison at different pulsed Nd:Yag laser irradiation flounces, 20, 30, 40 and 50 mJ/cm^2 at room temperature. The value is found to be 2, 3, 5.1, 6.4 and 8.3, respectively.

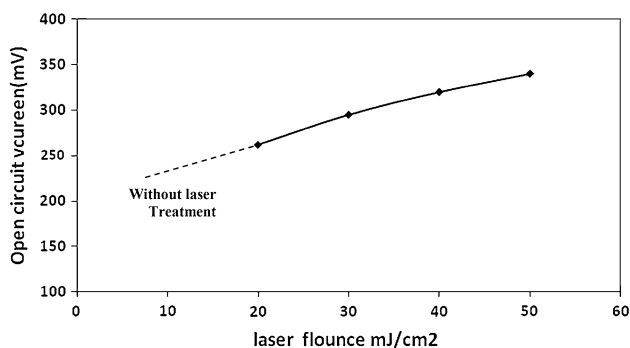**Fig. 5** I_{SC} as a function of laser flounce

Fig. 6 V_{OC} as a function of laser flounce

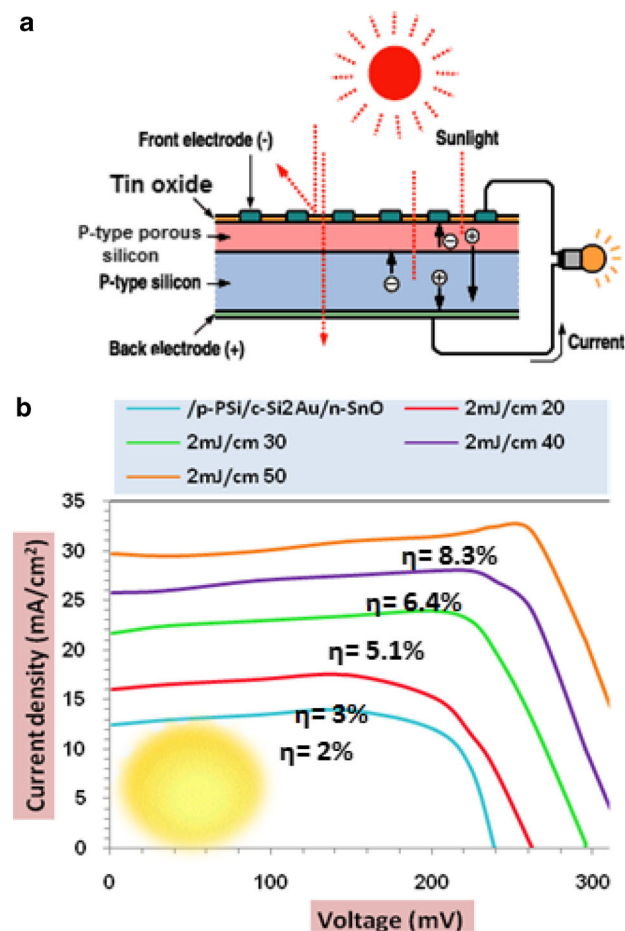Fig. 7 **a** Cross section of Au/SnO$_2$/PS/c-Si solar cell, **b** I–V characteristics of solar cell Au/SnO2/PS/c-Si devices at different pulsed Nd:Yag laser irradiation flounces, 20, 30, 40 and 50 mJ/cm^2 at room temperature

The improved value of quantum efficiency (QE) of irradiated samples is related to the reflection of light rays from one side to another, resulted in improved absorption, and therefore reduces reflection compared with crystalline Si surface [33] due to absorption phenomena in the surface oxide layer and at Au/SnO$_2$/PS/c-Si junction. Additionally,

Table 2 Obtained results from solar cell measurements

Au/SnO$_2$ /PS/c-Si Solar cell	I_m (mA)	V_m (mV)	I_{SC} (mA)	V_{OC} (mV)	FF (%)	η (%)
Without annealing	14	146.6	12.5	238.7	0.68	2
20 mJ/cm^2	15.2	201.5	16	262	0.73	3
30 mJ/cm^2	23	224.1	21.7	295	0.8	5.1
40 mJ/cm^2	27	238.7	25.8	320	0.78	6.4
50 mJ/cm^2	32	262	29.8	340	0.82	8.3

the interfacial porous silicon oxide (PSO$_2$) layer between PS and SnO$_2$ plays a significant role in enhancement of the properties; it has been found that the PS could be oxidized at high temperatures forming porous oxide layer. Increasing the laser flounces results in recrystallization of the crystalline structure that greatly enhances the heterojunction properties, due to the reduction of the trapping centers and crystalline defects, leading to an increase in photocurrent and solar cell efficiency. Heating of PS at high temperature leads to vary rapid oxidation of the structure. Rapid thermal oxidation (RTO) of PS makes it suitable as dielectric layer for any electronic device. Most of applications that involve the formation of stable SiO$_2$ layers obtained by technological process like thermal oxidation of PS at high temperature are conveniently carried out by RTO, involving transient heat of oxygen ambient so that careful control of potential rapid surface reaction can be maintained. The conversion efficiency and fill factor of solar cell are given in Table 2, using the following [31]:

$$\eta = \frac{p_m}{p_I} = \frac{I_m V_m}{P_i} \tag{3}$$

where P_m and P_i are the output and incident powers, respectively. The fill factor (FF) was calculated by [34]:

$$FF = \frac{I_m V_m}{I_{SC} V_{OC}} \tag{4}$$

where I_m is max output current, V_m is the max output voltage, I_{SC} is short-circuit current, and V_{OC} is short-circuit voltage.

4 Conclusions

SnO$_2$ nanostructures have been prepared on quartz and PS substrates using RTO of pure Sn at 600 °C and 90 s oxidation times. The lattice constants are investigated to be suitable for SnO$_2$ nanostructures. The grain size is measured precisely using SEM, and the porosity percentage 85 % is measured using weighting method. A significant enhancement was obtained by laser surface treatment with

different laser flounces. The outstanding solar cell efficiency of Au/n-SnO$_2$/p-PS/c-Si at 50 mJ/cm^2 is 8.3 %.

References

1. S. Yoshiaki, K. Hiroharu, I. Keitaro, O. Tamiko, Preparation of tin oxide (SnO2) thin film gas sensor by PLD method. Sci. Links Jpn. **123**, 222–227 (2003)
2. J. Joseph, V. Mathew, J. Mathew, K.E. Abraham, Studies on physical properties and carrier conversion of SnO2: Nd thin films. Turk. J. Phys. **33**, 37–47 (2008)
3. S. Wang, W. Wang, Q. Hu, Y. Qian, Surface modification of tin oxide ultrafine particle thin films. Mater. Res. Bull. **35**, 1235–1241 (2000)
4. S.M.A. Durrani, Biasing voltage dependence of sensitivity of electron beam evaporated SnO$_2$ thin film CO sensor. Sensors **6**, 1153–1160 (2006)
5. K. Zakrzewskaa, M. Radeckaa, J. Przewoźnika, K. Kowalskia, P. Czuba, Microstructure and photoelectrochemical characterization of the TiO$_2$–SnO$_2$ system. Thin Solid Films **490**, 101–107 (2005)
6. Y. Kim, J.-B. Yoon, J.-H. Choy, G. Campet, D. Camino, J. Portier, J. Salardenne, Rf sputtered SnO$_2$, Sn-doped In$_2$O$_3$ and Ce-doped TiO$_2$ films as transparent counter electrodes for electrochromic window. Bull. Korean Chem. Soc. **19**, 107–109 (1998)
7. H. Kato, T. Kanda, K. Yasuda, A. Yoshida, T. Arizumi, Electron beam irradiation effects on SnO$_2$–Si photodiodes. Phys. Status Solidi (a) **42**, 769–774 (2006)
8. D.M. Qu, P.X. Yan, J.B. Chang, D. Yan, J.Z. Liu, G.H. Yue, R.F. Zhuo, H.T. Feng, Nanowires and nanowire–nanosheet junctions of SnO$_2$ nanostructures. Mater. Lett. **61**, 2255–2258 (2007)
9. T.J. Stanimirova, P.A. Atanasov, I.G. Dimitrov, A.O. Dikovska, Investigation on the structural and optical properties of tin oxide films grown by pulsed laser deposition. J. Optoelectron. Adv. Mater. **7**, 1335–1340 (2005)
10. R. Khandelwal, Effects of deposition temperature on the structural and morphological properties of SnO$_2$ films fabricated by pulsed laser deposition. Opt. Laser Technol. **41**, 89–93 (2009)
11. J.E. Dominguez, X.Q. Pan, L. Fu, P.A. Van Rompay, Z. Zhang, J.A. Nees, P.P. Pronko, Epitaxial SnO$_2$ thin films grown on 1̄ 012 sapphire by femtosecond pulsed laser deposition. J. Appl. Phys. **91**, 1060–1065 (2002)
12. J.E. Dominguez, L. Fu, X.Q. Pan, Effect of crystal defects on the electrical properties in epitaxial tin dioxide thin films. Appl. Phys. Lett. **81**, 5163–5170 (2002)
13. U. Pal, A. Pérez-Centeno, M. Herrera-Zaldívar, Cathodoluminescence defect characterization of hydrothermally grown SnO2 nanoparticles. J. Appl. Phys. **103**, 1–6 (2008)
14. J.-H. Leea, G.-E. Janga, D.-H. Yoonb, S.-H. Sonc, Effect of deposition temperature on electro-optical properties of SnO2 thin films fabricated by a PECVD method. J. Ceram. Process. Res. **8**, 59–63 (2007)
15. A. Uhlir, Electrolytic Shaping of Germanium and Silicon. Bell Syst. Tech. J. **35**, 333–347 (1956)
16. Z. Gaburro, N. Daldosso, L. Pavesi, Porous silicon, in *Encyclopedia of Condensed Matter Physics*, ed. by F. Bassani, J. Liedl, P. Wyder (Elsevier, Oxford, 2005), pp. 391–401
17. B. Astuti, N. Rusli, A. Hashim, Z. Othaman, N. Nafarizal, N. Ali, N. Safi, Morphological and optical characteristics of porous silicon structure formed by electrochemical etching. AIP Conf. Proc. **1341**, 119–125 (2010)
18. L. Canham, Silicon quantum wire fabrication by electrochemical and chemical dissolution of wafers. Appl. Phys. Lett. **57**, 1046–1058 (1990)
19. J. Xu, A. Steckl, Visible electroluminescence from stain-etched porous Si diodes. Electron Device Lett. **15**, 507–513 (1994)
20. A. Ramizy, Z. Hassan, K. Omar, Y. Al-Douri, M.A. Mahdi, New optical features to enhance solar cell performance based on porous silicon surfaces. Appl. Surf. Sci. **257**, 6112–6117 (2011)
21. A. Alwan, A. Jabbar, Design and fabrication of nanostructures silicon photodiode. Mod. Appl. Sci. **5**, 106–115 (2011)
22. V. Yu, I. Sieber, J. Rappich, B. Kamene, P. Kashkarov, Laser-induced melting of porous silicon. Phys. Status Solidi (a) **182**, 325–333 (2000)
23. A. Chistyakov, V. Karavanski, M. Kuznetsov, G. Voronkova, V. Zuev, L. Orlova, On the possibility of controlling the photoluminescence spectrum of nanoporous silicon with laser radiation. AIP Conf. Proc. **10**, 881–889 (2000)
24. E.T. Salim, M.A. Muhsien, I.R. Agool, Construction of SnO2/SiO2/Si Heterojunction and its lineup using I–V and C–V measurements. Int. J. Mod. Phys. B **25**, 3863–3869 (2011)
25. J.A. Ayllon, M. Lira-Cantu, Application of MEH-PPV/SnO2 bilayer as hybrid solar cell. Appl. Phys. A **95**, 249–255 (2009)
26. Ü. Kersen, The gas-sensing potential of nanocrystalline SnO2 produced by a mechanochemical milling via centrifugal action. Appl. Phys. A **75**, 559–563 (2002)
27. T. Omata, H. Fujiwara, S. Otsuka-Yao-Matsuo, N. Ono, Electron trapping center and SnO$_2$-doping mechanism of indium tin oxide. Appl. Phys. A **71**, 609–614 (2000)
28. P.N. Patel, V. Mishra, A.K. Panchal, Synthesis and characterization of nano scale porous silicon photonic crystals for optical device and sensing applications. J. Optoelectron. Biomed. Mater. **4**, 19–28 (2012)
29. Marwa Abdul Muhsien, Evan T. Salem, Ibrahim R. Agool, Haidar Hamed Hamdan, Gas sensing of Au/n-SnO2/p-PSi/c-Si heterojunction devices prepared by rapid thermal oxidation. Appl. Nanosci. **4**, 719 (2014)
30. Y. Hubarevich, F. Wang, X. Sun, A. Smirnov, Thin porous silicon fabricated by electrochemical etching in novel ammonium fluoride solution for optoelectronic applications, in: Photonics Global Conference, Singapore (2010) pp. 14–16
31. E.T. Salim, M.A. Muhsien, I.R. Agool, Optical and electrical properties of SnO$_2$ thin film prepared using RTO method. Int. J. Mod. Phys. B **25**, 1081–1089 (2011)
32. J. Diana, A. Macek, D. Niznansky, I. Nemec, V. Vrkoslav, T. Chvojka, I. Jelınek, Appl. Surf. Sci. **238**, 169174 (2004)
33. E.T. Salim, Surface morphology and X-ray diffraction analysis for silicon nanocrystal based heterostructures. Surf. Rev. Lett. **20**, 1350046–1350052 (2013)
34. K.A. Salman, Z. Hassan, Khalid Omar. Int. J. Electrochem. Sci. **7**, 376–386 (2012)